

Dzyaloshinskii-Moriya Interaction-Induced Magnetoelectric Coupling in a tetrahedral Molecular Spin-Frustrated System

Jie-Xiang Yu,¹ Jia Chen,¹ Neil Sullivan,² and Hai-Ping Cheng^{1,*}

¹*Department of Physics, Center for Molecular Magnetic Quantum Materials and Quantum Theory Project, University of Florida, Gainesville, Florida 32611, USA*

²*Department of Physics and Center for Molecular Magnetic Quantum Materials, University of Florida, Gainesville, Florida 32611, USA*

We have investigated magnetoelectric coupling in the single-molecule magnet $\text{Mn}_4\text{Te}_4(\text{PET}_3)_4$ with tetrahedral spin frustration. Our density functional studies found that an electric dipole moment can emerge with various non-collinear spin orderings. The forms of spin-dependent dipole are determined and consistent with that in non-centrosymmetric magnets driven by the Dzyaloshinskii-Moriya interaction. Writing a parameterized spin Hamiltonian, after solving for eigenvalues and eigenstates we quantified the magnetoelectric coupling by calculating the thermal average of the electric and magnetic susceptibilities, which can be influenced by external magnetic and electric fields, respectively. The quadratic relations are expected to be observable in experiments.

I. INTRODUCTION

Considerable interest has been focused recently in the literature [1–6] on the search for multi-functional materials that couple magnetic and electric states through magneto-electric (ME) interactions. Interest is not only for the fundamental science but also for the possible generation of new electric-field-driven devices and their inherent low power dissipation compared to magnetically driven state changes found in conventional memory and related storage systems. In the search for new magnetoelectric materials it is important to note that ME effects accompany both time-reversal and spatial inversion symmetry breaking. For example, the lattice-mediated ME effect usually happens when controllable ferroelectric properties without centrosymmetry coexist with a structure sensitive spin state or spin ordering when time-reversal symmetry is broken. The distortion of the lattice influences both electric polarization and magnetic magnetism. Besides conventional crystalline solids, such ME effects based on ionic displacement have also been confirmed in molecule-based magnetic materials with lower Young's modulus [7–12].

Another origin of ME effect is the non-collinear magnetism characterized by the Dzyaloshinskii-Moriya (DM) interaction [13, 14] in non-centrosymmetric magnets. In this theory, the polarization is described by $\hat{\mathbf{e}}_{ij} \times (\mathbf{S}_i \times \mathbf{S}_j)$ where $\mathbf{j}_{ij} = \mathbf{S}_i \times \mathbf{S}_j$ is the so-called spin supercurrent for two spins \mathbf{S}_i and \mathbf{S}_j and $\hat{\mathbf{e}}_{ij}$ is the unit vector connecting the two spins [1, 15, 16]. The mechanism of DM-induced ME effect is confirmed in some spiral magnetic system such as rare-earth manganite TbMnO_3 and DyMnO_3 [17]. Although experiments found non-structural induced ME effects in some polynuclear molecular nanomagnets [18, 19], DM-induced ME effect studies in molecular magnets remain largely under-investigated. Special quantum features of the quantum spin states in

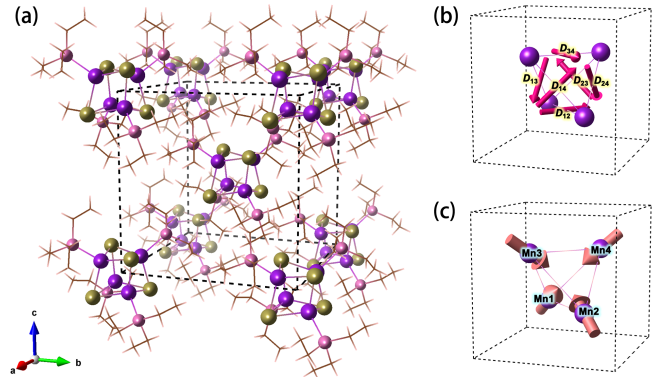


Figure 1. (a) The crystalline phase of $\text{Mn}_4\text{Te}_4(\text{PET}_3)_4$. Purple: Mn, dark yellow: Te, pink: P. (b) The DM vectors and (c) the axis of magnetic anisotropy in $\text{Mn}_4\text{Te}_4(\text{PET}_3)_4$.

molecular magnets that differentiate these systems from other crystalline materials can provide new ME couplings with potential applications in quantum information science.

When we consider the symmetry of a molecular magnet, tetrahedral symmetry with point group T (chiral tetrahedral symmetry) is a rare example in which the absence of spatial inversion symmetry alone does not bring about a net polarization. Furthermore, an anti-ferromagnetic exchange interaction in a tetrahedral geometry can lead to frustrated spins, where the ground spin state can be uncertain and easily be altered by external fields. A representative multiferric crystal system with tetrahedral structure is Cu_2OSeO_3 which hosts magnetically induced polarization in the ferrimagnetic, helimagnetic, and skyrmion crystal phases [20–24] because of DM interaction. In contrast to the distorted Cu_4 tetrahedron that does not respect tetrahedral spin frustration, the $\text{Mn}_4\text{Te}_4(\text{PET}_3)_4$ molecule where the magnetic center Mn_4 forms an equilateral tetrahedron in this study is a magnetically frustrated unit. The crystalline phase of $\text{Mn}_4\text{Te}_4(\text{PET}_3)_4$ shown in Fig. 1 has a body-

* hping@ufl.edu

centered-cubic lattice and the space group is $I23(197)$ with point group T , so that both the global symmetry and local chemical environment respect a perfect tetrahedral symmetry.

In this article, we have investigated both the magnetic properties and the electric polarization for various spin states of $\text{Mn}_4\text{Te}_4(\text{PET}_3)_4$ based on density functional calculations. We confirmed the DM-induced ME effect in the molecular magnets. After solving the eigenvalues and eigenstates of the parameterized spin Hamiltonian, we quantified the magnetoelectric coupling by calculating the thermal average of the electric susceptibility, which can be influenced by external magnetic field. The rest of the paper is organized as follows: In Section II, we describe the computational details; in Section III, we present results from DFT calculation and model Hamiltonian; and finally in Section IV, we conclude our investigation.

II. COMPUTATIONAL METHODS

Our density functional theory (DFT)-based calculations are performed with projector augmented wave pseudopotentials [25, 26] implemented in the Vienna ab initio simulation package (VASP) [27, 28]. The generalized gradient approximation (GGA) in the Perdew, Burke, and Ernzerhof (PBE) form [29] is used as the exchange-correlation energy, and the Hubbard U method ($U = 4.0\text{ eV}$, $J = 0.9\text{ eV}$) with density only and a spin-independent double counting scheme [30] is applied on $\text{Mn}(3d)$ orbitals to include strong-correlation effects. An energy cutoff of 600 eV is used for the plane-wave expansion throughout the calculations. The DFT-D3 method [31] with inclusion of van der Waals correction is employed. For non-collinear spin orderings, spin-orbit couplings (SOC) are included. The polarization vectors were obtained by the evaluation of the Berry phase expressions [32, 33].

We use a body-centered cubic lattice with experimental lattice constant 13.174 \AA [34] including one $\text{Mn}_4\text{Te}_4(\text{PET}_3)_4$ molecule for all calculations. The K -points were sampled on a $7 \times 7 \times 7$ Γ -centered mesh in the Brillouin zone.

III. RESULTS

A. Density functional results

DFT results showed that the local magnetic spin moment on each Mn is $4.27\mu_B$ in a collinear spin configuration where two of four Mn spins are up and other two are down, without spin-orbit coupling. As shown in Fig. 2(a), the total density-of-states (DOS) has a gap about 1.5 eV, indicating an insulating nature. The corresponding projected density-of-states (PDOS) results (see Fig. 2(b)) show that all $\text{Mn}(3d)$ components in the

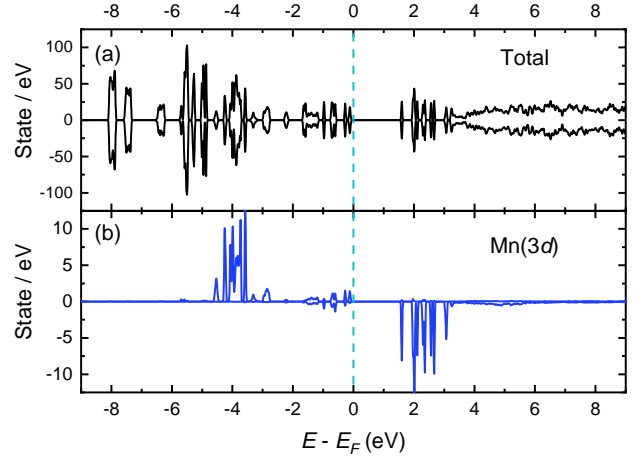


Figure 2. Without spin-orbit coupling: (a) the total density-of-states of $\text{Mn}_4\text{Te}_4(\text{PET}_3)_4$ in the two-up-two-down spin configuration. (b) The PDOS for $\text{Mn}(3d)$ orbitals. Positive and negative values refer to spin-majority channel and spin-minority channel, respectively. The Fermi energy is set to zero.

spin-majority channel are fully occupied while almost all $\text{Mn}(3d)$ components in the spin-minority are above the Fermi energy. Thus, each Mn ion has five spin-up electrons half filling the d orbitals, following Hund's rule, and in $\text{Mn}_4\text{Te}_4(\text{PET}_3)_4$, each Mn displays a +2 valence state and $S = 5/2$ high spin state. Before building a spin Hamiltonian, we point out that our calculations indicate that in this system the strain effect is negligible.

Because of the absence of inversion symmetry, the exchange interaction between two local magnetic spins on Mn includes an off-diagonal contribution, the Dzyaloshinskii-Moriya (DM) interaction [13, 14]. The strength of the DM interaction is proportional to the strength of SOC of the bridging Te, and is not negligible. The spin-spin Hamiltonian that properly includes this interaction for the four $S = 5/2$ spins on Mn^{2+} ions with tetrahedral symmetry is given by:

$$\mathcal{H}_0 = \sum_{\langle i,j \rangle} [J \mathbf{S}_i \cdot \mathbf{S}_j + \mathbf{D}_{ij} \cdot (\mathbf{S}_i \times \mathbf{S}_j)] - K_u \sum_i (\mathbf{M}_i \cdot \mathbf{S}_i)^2 \quad (1)$$

where J is the Heisenberg interaction and $\mathbf{D}_{ij} = D \hat{\mathbf{D}}_{ij}$ is the DM vector for two local spins on neighboring Mn sites i and j . Following Moriya's rule [14], the direction $\hat{\mathbf{D}}_{ij}$ is perpendicular to the Mn-Mn bond (see Fig. 2(b)). K_u is the magnitude of magnetic anisotropy (note that K_u is often denoted as D in molecular magnet literature) and \mathbf{M}_i is a unit vector which represents the direction of the magnetic anisotropy on Mn site i . Because of the tetrahedral symmetry, \mathbf{M}_i is directed from Mn site i to the body center of tetrahedron (see Fig. 2(c)).

Based on the Hamiltonian, we investigate the magnetic properties of $\text{Mn}_4\text{Te}_4(\text{PET}_3)_4$ by calculating total energies for two collinear spin configurations along the

[111] direction of the cubic crystalline lattice, all-up and two-up-two-down, and twelve non-collinear spin configurations, labeled SO1 to SO12, including six zero magnetization configurations and six non-zero magnetization configurations, shown in Fig. 3. The relative total energies are listed in Table I. We transfer spin configurations into quantum spin states. For each spin configuration α , each local magnetic spin i on Mn^{2+} has a normalized classical spin vector $\mathbf{e}_i = (e_{ix}, e_{iy}, e_{iz})$ and the spin quantum number $s_i = 5/2$. Diagonalizing the spin matrix $\mathbf{e}_i \cdot \mathbf{S}_i$ where \mathbf{S}_i is the matrix of the spin operator, we obtain the quantum spin state for this spin in the basis of $|s_{iz}\rangle$ which is the eigenvector $|\alpha_i\rangle$ with the eigenvalue $+5/2$. Therefore, the quantum spin state for this spin configuration is $|\alpha\rangle = |\alpha_1\rangle \otimes |\alpha_2\rangle \otimes |\alpha_3\rangle \otimes |\alpha_4\rangle$. Then the super-rank linear equations based on all spin configurations are

$$\{E_\alpha = E_0 + \langle \alpha | \mathcal{H}_0 | \alpha \rangle\}_\alpha \quad (2)$$

$$\begin{aligned} \langle \alpha | \mathcal{H}_0 | \alpha \rangle = & J \sum_{\langle i,j \rangle} \langle \alpha | \mathbf{S}_i \cdot \mathbf{S}_j | \alpha \rangle \\ & + D \sum_{\langle i,j \rangle} \langle \alpha | \hat{\mathbf{D}}_{ij} \cdot (\mathbf{S}_i \times \mathbf{S}_j) | \alpha \rangle \\ & - K_u \sum_i \langle \alpha | (\mathbf{M}_i \cdot \mathbf{S}_i)^2 | \alpha \rangle \end{aligned} \quad (3)$$

where E_α is the total energy of spin configuration α and E_0 is the spin-irrelevant energy. The parameters J , D , and K_u are then obtained from energy fitting. According to a suggestion of Ruiz *et al.* [35, 36], when the spin broken symmetric antiferromagnetic spin ordering includes overlapped occupied molecular orbitals, a correction of $1 + \min(S_i, S_j)/2S_i S_j$ is included for obtaining the expectation values of the exchange interaction terms. The solution according to a least-square fit leads to $J = 14.02$ meV, $D = -0.44$ meV, and $K_u = 0.26$ meV. Positive J indicates antiferromagnetic coupling. A negative D gives an opposite direction of spiral direction compared to a positive one. Positive K_u means that each \mathbf{M}_i of site i is an easy axis.

The electric dipole moments are calculated for each spin configuration. According to the results shown in Table I, both collinear spin configurations and all six non-collinear configurations with zero magnetization have zero dipole moment. Among non-collinear configurations from SO7 to SO12, SO7 has a non-zero electric dipole moment $0.012 e\text{\AA}$ along the [100] direction, the same as the direction of its net magnetization. Spin configurations SO8 and SO11, with the same magnetization along the [100] direction, provide an electric dipole of the same magnitude $0.019 e\text{\AA}$ and opposite orientations along the [101] direction. Both SO9 and SO12 retain a three-fold rotation axis along the [111] direction with non-zero magnetization and dipole moment $0.058 e\text{\AA}$ along the same direction. Configuration SO10 has zero electric dipole moment. All dipole moments are plotted in Fig. 3. Note

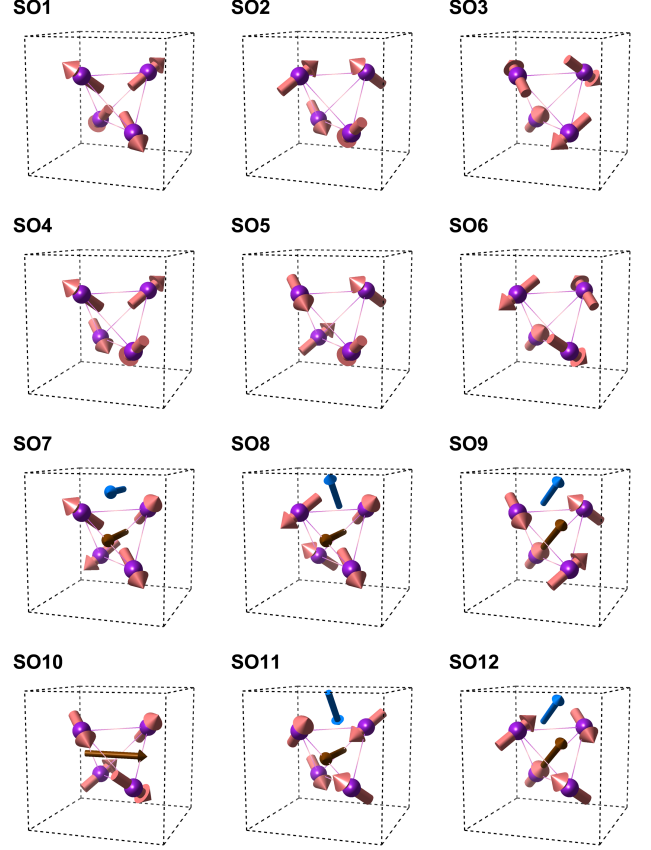


Figure 3. Twelve non-collinear spin configurations, labeled SO1 to SO12, used for total energy calculations and electric dipole calculations. Brown and blue arrows corresponds to the directions of the total magnetization and the electric dipole moment for each spin configuration, respectively.

that the atomic positions as well as the lattice are fixed, so that the calculated dipole moments are purely from charge density displacement driven by non-collinear spin ordering, indicating a magnetoelectric coupling. The dipole moments are not changed significantly when the atomic positions are relaxed in their spin configurations. The spin-driven magnetoelectric coupling is robust.

The spin-dependent electric dipole moments do not change magnitude or sign when all spins are reversed, indicating that the dipole is a function of even order in spins. SO11 is the spin configuration where spins on Mn1 and Mn2, Mn3 and Mn4 are exchanged from SO8, reversing the direction of the dipole moment. Furthermore, SO9 and SO12, with opposite spin chiralities, result the same dipole moment, so the dipole moment is not relevant to chiral spin textures. Based on the dipole moment results from DFT and analysis based on symmetry properties, we obtain the spin-dependent electric dipole moment as a function of spins as,

$$\mathbf{P} = \alpha \sum_{\langle i,j \rangle} \hat{\mathbf{e}}_{ij} \times (\mathbf{S}_i \times \mathbf{S}_j) \quad (4)$$

Table I. The relative total energies and the magnitude of the dipole moment for each spin configuration. SO1-SO12 correspond to the non-collinear spin configurations shown in Fig. 3. CO-uudd and CO-uuuu correspond to two collinear configuration along the [111] direction of the cubic crystalline lattice, all-up and two-up-two-down, respectively.

	E (meV)	P (eÅ)
SO1	0.00	0.000
SO2	-20.80	0.000
SO3	-17.32	0.000
SO4	-24.27	0.000
SO5	-9.17	0.000
SO6	-17.3	0.000
SO7	275.94	0.012
SO8	265.13	0.019
SO9	208.24	0.058
SO10	276.83	0.000
SO11	265.13	0.019
SO12	208.24	0.058
CO-uudd	12.11	0.000
CO-uuuu	946.43	0.000

where $\hat{\mathbf{e}}_{ij}$ is the direction from site i to j . The magnitude of the coefficient α is about $0.005 - 0.035 \text{ eÅ}$ in $\text{Mn}_4\text{Te}_4(\text{PEt}_3)_4$ based on different spin configurations with non-zero spin-dependent electric dipole moment. Here we demonstrate that even at the single molecular scale, the DM-induced ME effect is still valid.

We also investigated the magnetic and dielectric properties under hydraulic external strain by modulating the lattice constant. As a result, both no significant response of the relative total energies is identified, and dipole moments for the spin configurations are almost invariant. This indicates that the ME effect are insensitive to strain.

B. Quantum spin model

Once the spin-dependent electric dipole moment is determined, the Hamiltonian for the response to external magnetic field and electric field is given by

$$\mathcal{H} = \mathcal{H}_0 - \mathbf{B} \cdot \sum_i \mathbf{S}_i - \mathbf{E} \cdot \mathbf{P} \quad (5)$$

where $b\mathbf{m}\mathbf{E}$ is the electric field, \mathbf{P} is the spin-driven polarization, and $\mathbf{B} = g\mu_B\mu_0\mathbf{H}$ is proportional to the magnetic field \mathbf{H} . The electric field is coupled with spins since the electric dipole moment is a function of spin as in eq. (4), with $\alpha = 0.035 \text{ eÅ}$ chosen. We diagonalized the Hamiltonian matrix for various \mathbf{B} and \mathbf{E} and obtained the total $6^4 = 1296$ eigenvalues and eigenstates. The corresponding quantum spin states and the expectation values of polarization are also obtained.

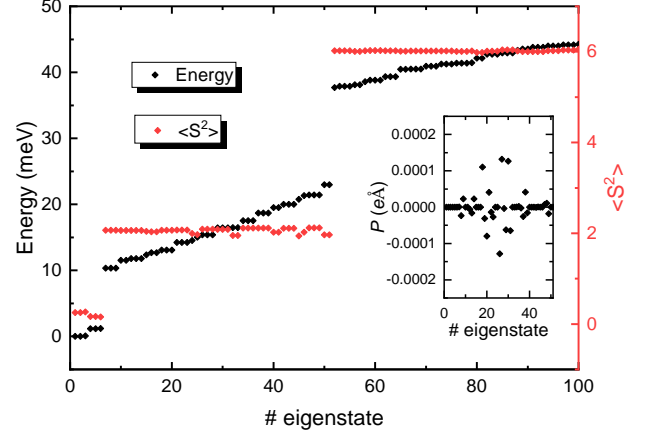


Figure 4. Without external magnetic and electric fields, the eigenvalues (energies) and the expectation value of $\langle S^2 \rangle$ of the first 100 eigenstates. The energy of the ground state is set to zero. Insert: the expectation value of the dipole moment for the first 51 eigenstates.

The eigenvalues and the expectation value of $\langle S^2 \rangle$ of the first 100 eigenstates Under zero magnetic and electric field are shown in Fig. 4. Note that because of the DM interaction in the Hamiltonian, the total spin S of the molecule is not a good quantum number and the expectation value of $\langle S^2 \rangle$ is not precisely $S(S+1)$ for each eigenstate. However, since $D \ll J$ in $\text{Mn}_4\text{Te}_4(\text{PEt}_3)_4$, the integer spin quantum number can still be used to label the spin states. The first six eigenstates with the lowest energies have $\langle S^2 \rangle$ close to zero, so that these states correspond to a $S = 0$ quantum spin state. The next 45 states, which are about 10 meV higher than the $S = 0$ states, have $\langle S^2 \rangle$ near 2, corresponding to a $S = 1$ state. The final 49 eigenstates are about 40 meV higher than $S = 0$ states and have $\langle S^2 \rangle$ near 6, corresponding to a $S = 2$ state. Considering that the energy scale of external fields is several meV, we focus on $S = 0$ and $S = 1$ states.

The results of expectation values of polarization for $S = 0$ and $S = 1$ states are shown in the insert of Fig. 4. All six of the $S = 0$ states have zero dipole moment. Some $S = 1$ states have a non-zero polarization, but the magnitude of the dipole moment is much smaller than the non-zero dipole obtained from DFT calculations. It is because that according to the DFT results, the spin configurations with non-zero dipole such as SO9 and SO12 have non-zero total magnetization and are more than 200 meV higher in energy than the spin configurations with zero magnetization. Therefore, the quantum spin states $S = 1$, the superposition of classical spin configurations, are dominated by zero magnetization configurations and only have very small non-zero dipole moment.

Based on the eigenvalues, eigenstates, and the corresponding expectation values of spins and dipoles of quan-

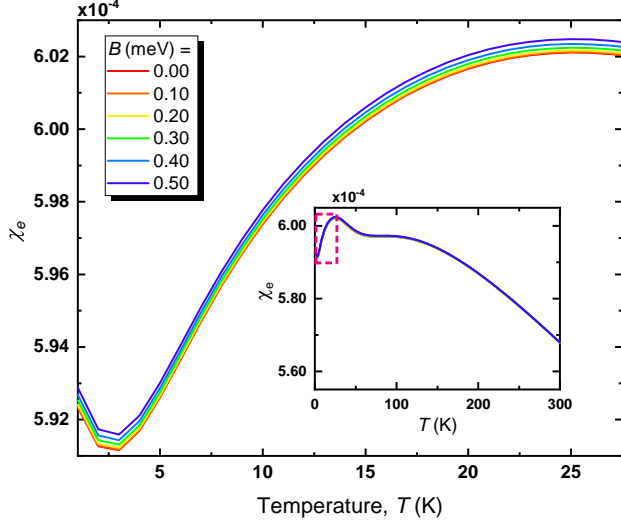


Figure 5. The electric susceptibility as a function of temperature with various magnetic fields. The red dashed rectangle in the insert panel shows the region expanded in the main panel. The direction of electric susceptibility is perpendicular to the direction of magnetic field (along c -axis in Fig. 1(a)).

tum spin model, we obtained thermal properties of that system. The corresponding partition function Z , thermal average of magnetization $\bar{\mathbf{m}}$ and dipole $\bar{\mathbf{P}}$ at finite temperature $\beta = 1/k_B T$ are given by

$$Z(\mathbf{E}, \mathbf{B}, \beta) = \sum_i \exp(-\beta \varepsilon_i) \quad (6)$$

$$\bar{\mathbf{m}}(\mathbf{E}, \mathbf{B}, \beta) = \frac{g\mu_B}{Z} \sum_i \langle \mathbf{S} \rangle \exp(-\beta \varepsilon_i) \quad (7)$$

$$\bar{\mathbf{P}}(\mathbf{E}, \mathbf{B}, \beta) = \frac{1}{Z} \sum_i \langle \mathbf{P} \rangle \exp(-\beta \varepsilon_i) \quad (8)$$

where the summation is over all eigenvalues $\{\varepsilon_i\}$. Then the corresponding electric susceptibility χ_e which depends on magnetic fields is given by

$$\chi_e(\mathbf{E}, \mathbf{B}, \beta) = \frac{\partial \bar{\mathbf{P}}(\mathbf{B}, \mathbf{E})}{\partial \mathbf{E}}. \quad (9)$$

Similarly, the magnetic susceptibility χ_m influenced by electric fields is given by

$$\chi_m(\mathbf{E}, \mathbf{B}, \beta) = \frac{\partial \bar{\mathbf{m}}(\mathbf{B}, \mathbf{E})}{\partial \mathbf{B}}. \quad (10)$$

The temperature dependent results for χ_e and χ_m are shown in Fig. 5 and Fig. 6, respectively. In the inserts for both χ_e and χ_m , dashed contours identify the region of non-zero magnetoelectric response, where χ_e can be affected by magnetic fields and χ_m is modulated by the electric fields, though the magnitude of magnetoelectric coupling is very small.

All the electric susceptibility curves have a local minimum at $T \sim 3$ K and a local maximum at $T \sim 25$ K.

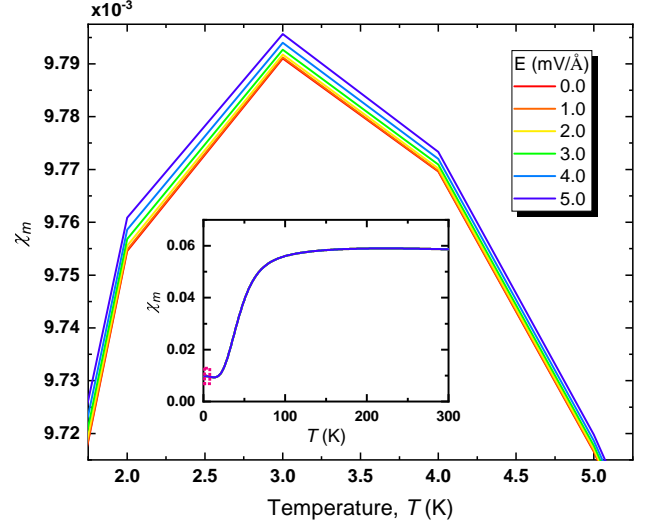


Figure 6. The magnetic susceptibility as a function of temperature with various electric fields. The red dashed rectangle in the insert panel shows the region expanded in the main panel. The direction of magnetic susceptibility is perpendicular to the direction of electric fields (along b -axis in Fig. 1(a)).

Meanwhile, all the magnetic susceptibility curves have a local maximum about at $T \sim 3$ K and a local minimum at $T \sim 25$ K. Since the energy of about 2.2 meV corresponding to 25 K is much smaller than the energy gap between $S = 0$ and $S = 1$ states, the thermal average of χ_e and χ_m below 25 K is determined by only the first six $S = 0$ states. For each eigenstate i , the contribution to χ_m is proportional to the fluctuation of spins $\langle \mathbf{S}^2 \rangle - \langle \mathbf{S} \rangle^2$, and $\langle \mathbf{S} \rangle = 0$ when $B = 0$, so that $\chi_m^{(i)} \propto \langle \mathbf{S}^2 \rangle$. Therefore, at finite temperature $\chi_m \propto \sum_i \langle \mathbf{S}^2 \rangle \exp(-\beta \varepsilon_i)$. The $\langle \mathbf{S}^2 \rangle$ values of the first six eigenstates are 0.251, 0.251, 0.269, 0.166, 0.166, 0.158 from low to high eigenvalues respectively. The third eigenstate, with the highest $\langle \mathbf{S}^2 \rangle$ among the six $S = 0$ states, is only 0.09 meV (1.04 K) higher than the doubly degenerate ground states. This leads to the small peak of χ_m at $T \sim 3$ K. On the other hand, the three higher eigenstates with a gap about 1.18 meV (13.7 K) above the ground states have lower $\langle \mathbf{S}^2 \rangle$ than the three lower eigenstates. This leads to the small valley in χ_m at $T \sim 25$ K. Then, above $T \sim 50$ K, a rise in χ_m appears as temperature increases. This is because, as temperature increases, more $S = 1$ states contribute to an increase in $\langle \mathbf{S}^2 \rangle$. Note that the antiferromagnetic character is robust for all the temperature region up to 300 K, so that χ_m does not follow the paramagnetic behavior $\chi_m \propto 1/T$.

To further investigate the magnetoelectric coupling, we obtained the change of χ_e as a function of B and the change of χ_m as a function of E , shown in Fig. 7. The fitted dotted lines show a robust quadratic relation, so that $\chi_e \sim B^2$ and $\chi_m \sim E^2$. Since the magnetoelectric coupling originates from the dipole moment term, which

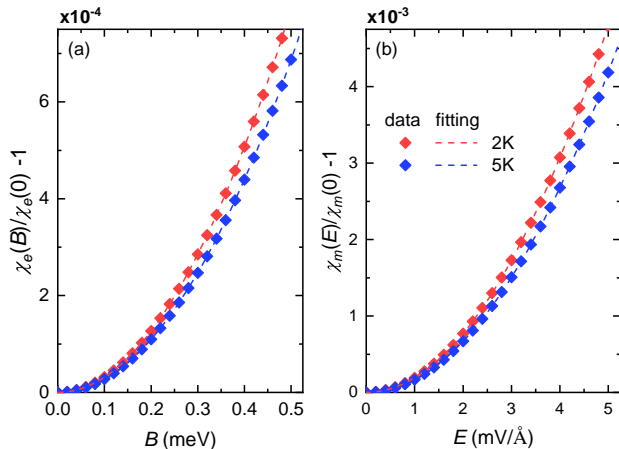


Figure 7. At 2 K and 5 K, (a) the change of electric susceptibility as a function of magnetic field B and (b) the change of magnetic susceptibility as a function of electric field E . Solid diamonds are the data and Dashed lines are the results of quadratic fitting.

involves the cross product of two spins, the quadratic relation is the leading order, with zero linear term according to linear response theory. Further, the quadratic relations mean that the inversion of magnetic/electric fields leaves invariant χ_e/χ_m . It is also consistent with the DFT result that flipping spins leaves the total dipole moment invariant.

The magnitude of magnetoelectric coupling from the quantum spin model is much smaller than that found from the DFT calculations. The reason is the quantum spin in a finite system. In contrast to frustrated systems in solids where magnetic spins are regarded as classical spin vectors, spins of frustrated systems in molecular magnets often exhibit their quantum nature. In solids, spin vectors can rotate continuously with external fields, since the system is gapless. In a quantum spin system, there is a gap between different quantum spin states and the magnitude of the gap is positively correlated the the magnitude of the exchange interaction, DM interaction, and magnetic anisotropy. Once the energy of the external field is much smaller than the gap, the response is limited.

C. Implication for experimental measurements

Fig. 7(b) shows the predicted change in spin susceptibility for experimentally accessible E fields. The fractional change in magnetic susceptibility at 2 K for $E = 0.10 \text{ V/\AA}$ (or 1 MV/m) is

$$\frac{\Delta\chi_m(E)}{\chi_m(0)} \approx 3 \times 10^{-6}. \quad (11)$$

Although the change is very small, it is within the range of modern high sensitivity techniques for measuring radio frequency susceptibility [37]. For typical experimental applied field strengths of order of $3 \times 10^5 \text{ V m}^{-1}$, the fractional change in the magnetic susceptibility is $\Delta\chi_m(E)/\chi_m(0) \approx 2 \times 10^{-7}$ which is comparable to experimental capabilities of the order of 1×10^{-7} in the relevant temperature range.

It is also significant that the dependence of the change in magnetic susceptibility on electric field strength is quadratic, as shown in Fig.7. The absence of a linear electric effect is due to the lack of large strain dependence. The magnetoelectric effect is caused by a superexchange interaction via Mn-Te-Mn, or symmetric striction. Because of the quadratic dependence on field strength, experiments should be designed for the highest possible values of E within limitations imposed by electrical breakdowns of sample cell materials and thermal bonding agents used for the samples.

IV. CONCLUSION

In summary, we first investigated the magnetic properties of the crystalline phase of $\text{Mn}_4\text{Te}_4(\text{PET}_3)_4$ based on first principles calculations. Each Mn has a $S = 5/2$ high spin state. The antiferromagnetic coupling leading to frustrated spins and the non-collinear DM interaction as well as the magnetic anisotropy was identified and quantized. A non-zero electric dipole moment was obtained in non-collinear spin configurations based on Berry phase calculations. The magnitude of the dipole moment follows the formula $\sim \hat{\mathbf{e}}_{ij} \times (\mathbf{S}_i \times \mathbf{S}_j)$. So that the electric dipole is coupled with non-collinear magnetic moment and we thus found the DM-induced ME effect in the single molecular scale. After parameterized the spin-spin Hamiltonian, we studied the quantum spin model based on the eigenvalues and eigenstates found by the direct diagonalization of the Hamiltonian. The magnetic susceptibility χ_m is changed by the electric field E and the electric susceptibility χ_e is changed by the magnetic field B , though the change is small. Further studies showed quadratic relations between both χ_m and E , and χ_e and B , respectively. Such ME effect is expected to be observable in experiments.

ACKNOWLEDGMENTS

This work is supported as part of the Center for Molecular Magnetic Quantum Materials, an Energy Frontier Research Center funded by the U.S. Department of Energy, Office of Science, Basic Energy Sciences under Award No. DE-SC0019330. Computations were performed at NERSC and the University of Florida Research Computer Center.

- [1] S.-W. Cheong and M. Mostovoy, Multiferroics: a magnetic twist for ferroelectricity, *Nature Materials* **6**, 13 (2007).
- [2] N. A. Spaldin, S.-W. Cheong, and R. Ramesh, Multiferroics: Past, present, and future, *Physics Today* **63**, 38 (2010).
- [3] S. Fusil, V. Garcia, A. Barthélémy, and M. Bibes, Magnetoelectric devices for spintronics, *Annual Review of Materials Research* **44**, 91 (2014).
- [4] M. Fiebig, T. Lottermoser, D. Meier, and M. Trassin, The evolution of multiferroics, *Nature Reviews Materials* **1**, 16046 (2016).
- [5] J.-P. Rivera, A short review of the magnetoelectric effect and related experimental techniques on single phase (multi-) ferroics, *The European Physical Journal B* **71**, 299 (2009).
- [6] H. Schmid, Magnetoelectric effects in insulating magnetic materials, in *Complex Mediums*, Vol. 4097, edited by A. Lakhtakia, W. S. Weiglhofer, and R. F. Messier, International Society for Optics and Photonics (SPIE, 2000) pp. 12 – 24.
- [7] S. Chikara, J. Gu, X.-G. Zhang, H.-P. Cheng, N. Smythe, J. Singleton, B. Scott, E. Krenkel, J. Eckert, and V. S. Zapf, Magnetoelectric behavior via a spin state transition, *Nature Communications* **10**, 4043 (2019).
- [8] J.-X. Yu, D.-T. Chen, J. Gu, J. Chen, J. Jiang, L. Zhang, Y. Yu, X.-G. Zhang, V. S. Zapf, and H.-P. Cheng, Three jahn-teller states of matter in spin-crossover system Mn(taa), *Physical Review Letters* **124**, 227201 (2020).
- [9] V. S. Zapf, P. Sengupta, C. D. Batista, F. Nasreen, F. Wolff-Fabris, and A. Paduan-Filho, Magnetoelectric effects in an organometallic quantum magnet, *Physical Review B* **83**, 140405 (2011).
- [10] M. Yazback, J.-X. Yu, S. Liu, L. Zhang, N. S. Sullivan, and H.-P. Cheng, First-principles study of an s=1 quasi one-dimensional quantum molecular magnetic material, *Physical Review B* **103**, 054434 (2021).
- [11] S. Chikara, J. Gu, X.-G. Zhang, H.-P. Cheng, Nathan, J. Singleton, B. Scott, E. Krenkel, J. Eckert, and V. S. Zapf, Magnetoelectric behavior via a spin state transition, *Nature Communications* **10**, 4043 (2019).
- [12] V. B. Jakobsen, S. Chikara, J.-X. Yu, E. Dobbelaar, C. T. Kelly, X. Ding, F. Weickert, E. Trzop, E. Collet, H.-P. Cheng, G. G. Morgan, and V. S. Zapf, Giant magnetoelectric coupling and magnetic-field-induced permanent switching in a spin crossover Mn(III) complex, *Inorganic Chemistry* **60**, 6167 (2021).
- [13] I. Dzyaloshinsky, A thermodynamic theory of “weak” ferromagnetism of antiferromagnetics, *Journal of Physics and Chemistry of Solids* **4**, 241 (1958).
- [14] T. Moriya, Anisotropic superexchange interaction and weak ferromagnetism, *Physical Review* **120**, 91 (1960).
- [15] H. Katsura, N. Nagaosa, and A. V. Balatsky, Spin current and magnetoelectric effect in noncollinear magnets, *Physical Review Letters* **95**, 057205 (2005).
- [16] H. Katsura, A. V. Balatsky, and N. Nagaosa, Dynamical magnetoelectric coupling in helical magnets, *Physical Review Letters* **98**, 027203 (2007).
- [17] T. Kimura, Spiral magnets as magnetoelectrics, *Annual Review of Materials Research* **37**, 387 (2007).
- [18] A. K. Boudalis, J. Robert, and P. Turek, First demonstration of magnetoelectric coupling in a polynuclear molecular nanomagnet: Single-crystal EPR studies of $[\text{Fe}_3\text{O}(\text{O}_2\text{CPh})_6(\text{py})_3]\text{ClO}_4 \cdot \text{py}$ under static electric fields, *Chemistry - A European Journal* **24**, 14896 (2018).
- [19] J. Robert, N. Parizel, P. Turek, and A. K. Boudalis, Polyanisotropic magnetoelectric coupling in an electrically controlled molecular spin qubit, *Journal of the American Chemical Society* **141**, 19765 (2019).
- [20] J. H. Yang, Z. L. Li, X. Z. Lu, M.-H. Whangbo, S.-H. Wei, X. G. Gong, and H. J. Xiang, Strong dzyaloshinskii-moriya interaction and origin of ferroelectricity in Cu_2OSeO_3 , *Physical Review Letters* **109**, 107203 (2012).
- [21] S. Seki, S. Ishiwata, and Y. Tokura, Magnetoelectric nature of skyrmions in a chiral magnetic insulator Cu_2OSeO_3 , *Physical Review B* **86**, 060403 (2012).
- [22] S. Seki, X. Z. Yu, S. Ishiwata, and Y. Tokura, Observation of skyrmions in a multiferroic material, *Science* **336**, 198 (2012).
- [23] J. S. White, K. Prša, P. Huang, A. A. Omrani, I. Živković, M. Bartkowiak, H. Berger, A. Magrez, J. L. Gavilano, G. Nagy, J. Zang, and H. M. Rønnow, Electric-field-induced skyrmion distortion and giant lattice rotation in the magnetoelectric insulator Cu_2OSeO_3 , *Physical Review Letters* **113**, 107203 (2014).
- [24] E. Ruff, P. Lunkenheimer, A. Loidl, H. Berger, and S. Krohns, Magnetoelectric effects in the skyrmion host material Cu_2OSeO_3 , *Scientific Reports* **5**, 15025 (2015).
- [25] P. E. Blöchl, Projector augmented-wave method, *Physical Review B* **50**, 17953 (1994).
- [26] G. Kresse and D. Joubert, From ultrasoft pseudopotentials to the projector augmented-wave method, *Physical Review B* **59**, 1758 (1999).
- [27] G. Kresse and J. Furthmüller, Efficiency of ab-initio total energy calculations for metals and semiconductors using a plane-wave basis set, *Computation Materials Science* **6**, 15 (1996).
- [28] G. Kresse and J. Furthmüller, Efficient iterative schemes for ab initio total-energy calculations using a plane-wave basis set, *Physical Review B* **54**, 11169 (1996).
- [29] J. P. Perdew, K. Burke, and M. Ernzerhof, Generalized gradient approximation made simple, *Physical Review Letters* **77**, 3865 (1996).
- [30] V. I. Anisimov, I. V. Solovyev, M. A. Korotin, M. T. Czyżyk, and G. A. Sawatzky, Density-functional theory and NiO photoemission spectra, *Physical Review B* **48**, 16929 (1993).
- [31] S. Grimme, J. Antony, S. Ehrlich, and H. Krieg, A consistent and accurate ab initio parametrization of density functional dispersion correction (DFT-d) for the 94 elements h-pu, *The Journal of Chemical Physics* **132**, 154104 (2010).
- [32] R. D. King-Smith and D. Vanderbilt, Theory of polarization of crystalline solids, *Physical Review B* **47**, 1651 (1993).
- [33] R. Resta, Macroscopic polarization in crystalline dielectrics: the geometric phase approach, *Reviews of Modern Physics* **66**, 899 (1994).
- [34] B. Choi, D. W. Paley, T. Siegrist, M. L. Steigerwald, and X. Roy, Ligand control of manganese telluride molecu-

- lar cluster core nuclearity, *Inorganic Chemistry* **54**, 8348 (2015).
- [35] E. Ruiz, J. Cano, S. Alvarez, and P. Alemany, Broken symmetry approach to calculation of exchange coupling constants for homobinuclear and heterobinuclear transition metal complexes, *Journal of Computational Chemistry* **20**, 1391 (1999).
- [36] E. Ruiz, A. Rodríguez-Forteza, J. Cano, S. Alvarez, and P. Alemany, About the calculation of exchange coupling constants in polynuclear transition metal complexes, *Journal of Computational Chemistry* **24**, 982 (2003).
- [37] A. Sirusi, J. Adams, M. Lewkowitz, R. Sun, and N. S. Sullivan, A tunnel diode oscillator for high sensitivity broad temperature range susceptibility measurements (2021), [arXiv:2109.11030 \[physics.ins-det\]](#).